Journal of Colloid and Interface Science 542 (2019) 23–32

Contents lists available at ScienceDirect

Journal of Colloid and Interface Science

journal homepage: www.elsevier.com/locate/jcis

Regular Article

Versatile reconfigurable glass capillary microfluidic devices with Lego® inspired blocks for drop generation and micromixing

Monalie V. Bandulasena, Goran T. Vladisavljević *, Brahim Benyahia *

Department of Chemical Engineering, Loughborough University, Loughborough LE11 3TU, United Kingdom

GRAPHICAL ABSTRACT

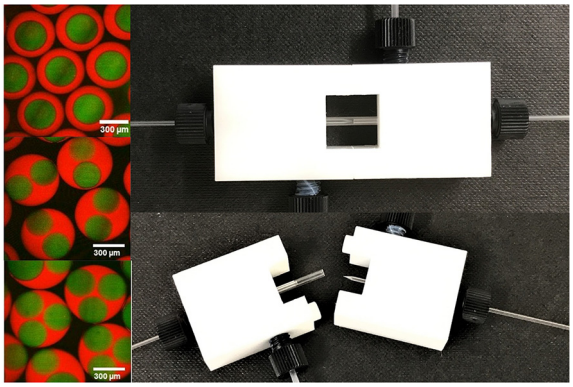

ARTICLE INFO

Article history:
Received 23 December 2018
Revised 25 January 2019
Accepted 28 January 2019
Available online 29 January 2019

Keywords:
Glass capillary microfluidics
CNC milling
Micromixing
Metal nanoparticles
Liposomes
Microfluidic antisolvent crystallisation

ABSTRACT

Novel cost effective, versatile, reconfigurable, reusable and easy to assemble glass capillary microfluidic devices were developed and used to generate micro/nano-materials with controlled size and morphology. The devices are composed of coaxial assemblies of glass capillaries held between two interchangeable plastic blocks fabricated from chemically inert polyoxymethylene copolymer using computer numerical control (CNC) machining. Three different blocks were combined and locked together using Lego® inspired stud-and-hole coupling system to achieve different flow configurations. The device allows a truly axisymmetric round capillary inside a round capillary geometry and self-alignment of capillaries. The synthesis of polyvinylpyrrolidone capped gold nanoparticles and liposomes of controlled size was demonstrated in the co-flow device by mixing the contents of two parallel laminar streams. The flow focusing device was used to generate piroxicam monohydrate crystals of controlled size (10–29 µm) by antisolvent crystallisation. Silver nanoparticles with tailored size (40–90 nm) were prepared in the three-phase device by merging silver nitrate and tannic acid/citrate streams inside droplets. The same device was used to prepare fluorescently labelled double emulsion droplets with controlled number of inner droplets. The droplet morphology was modified and tuned during operation by adjusting the distance between the inner capillaries. Water-in-oil emulsions consisted of Eudragit S100 solution at pH > 7 dispersed in Miglyol® 840 were prepared and gellified *in situ* over 6 h without fouling. The setup time of the novel devices was reduced from ~30 min in manually made capillary devices to just several minutes.

* Corresponding authors.
E-mail addresses: g.vladisavljevic@lboro.ac.uk (G.T. Vladisavljević), b.benyahia@lboro.ac.uk (B. Benyahia).

https://doi.org/10.1016/j.jcis.2019.01.119
0021-9797/

Nomenclature

D	diffusion coefficient (m^2/s)
D_i	injection capillary orifice diameter (μm)
D_c	collection capillary orifice diameter (μm)
D_d	droplet diameter (μm)
D_p	particle diameter (nm)
D_v	vesicle size (nm)
L	length of mixing (m)
ΔL	distance between injection and collection capillary orifice (m)
Pe	Peclet number (/)
Q	volumetric flow rate (ml/h)
t	time (s)
t_{res}	residence time (s)
t_{mix}	mixing time (s)
λ_{max}	wavelength of maximum absorbance (nm)
μ	dynamic viscosity (Pa s)
ρ	density (kg/m^3)

Subscripts

w	aqueous phase
o	organic phase
cp	continuous phase
dp	dispersed phase
ip	inner phase
mp	middle phase
op	outer phase

1. Introduction

Microfluidics is one of the key microfabrication techniques to manipulate micro-, nano-, and pico-litre volumes of fluids inside micrometre-sized channels. Microfluidic technology has been widely and increasingly used for diagnostics, detection, screening, flow chemistry and materials synthesis in biotechnology and the chemical, food, pharmaceutical, and cosmetic industries [1–4].

Glass capillary microfluidic devices composed of coaxial assemblies of glass capillaries have received a lot of attention since their invention in Weitz Lab at Harvard [4,5], due to their ability to generate multiple emulsion droplets with core-shell morphology in single step by combining co-flow with counter current flow focusing. They can produce droplets with multiple concentric shells and can be used to encapsulate two or more different types of inner drops within the same outer drop by inserting several injection capillaries into the same outer capillary [6–8] or by using dual-, triple-, and quadruple-bore injection capillaries [9–11]. Glass capillary devices can also generate multiple emulsions stepwise [12–15] and form droplets with a submicron shell thickness by creating biphasic flow in the injection capillary [16].

Alternative methods for fabrication of microfluidic devices are etching, hot embossing, laser ablation, injection moulding, and soft lithography [17]. Soft lithography is a well-established method for rapid prototyping of microfluidic devices in polydimethylsiloxane (PDMS). However, PDMS is a hydrophobic polymer and inconvenient for preparing oil-in-water (O/W) emulsions [18]. In addition, organic solvents can cause PDMS swelling, extraction of unpolymerized monomers from PDMS matrix, permeation of hydrophobic solutes into the polymer matrix and chemical decomposition of PDMS [18,19]. Swelling can significantly alter dimensions of PDMS channels and even cause channel closure [20]. Extraction of non-crosslinked species can introduce contaminants into fluid streams and partitioning of solutes between fluids and cured PDMS can alter reagent concentrations. Unlike PDMS, glass is resistant to all reagents except hydrofluoric acid, hot concentrated phosphoric acid, and concentrated sodium hydroxide solutions, almost non-deformable with a Young's modulus of 64 kN/mm^2, highly transparent with a transmittance of visible light near unity, and can easily be chemically modified due to high reactivity of silanol groups.

PDMS and etched glass chips are difficult to clean because the etched substrate is permanently bonded to the cover glass. In traditional glass capillary devices [4], capillary tubes and needles for fluid delivery are sealed to the support glass slide using epoxy glue (Fig. 1a) and cannot be easily separated for cleaning. Moreover, fabrication of these devices is time consuming and laborious, since capillaries must be manually aligned.

To mitigate these limitations, several new designs of glass capillary devices have been developed. Li et al. [21] fabricated a disposable co-flow glass capillary device by embedding glass capillaries into a rectangular gap formed between two parallel

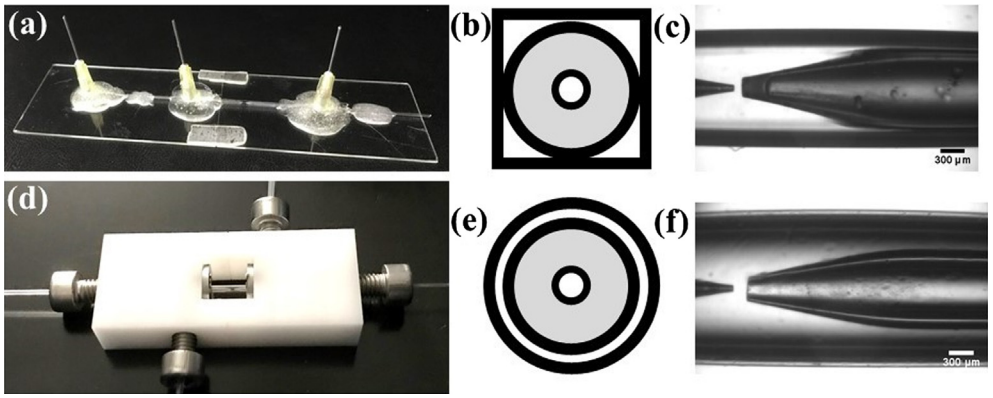

Fig. 1. Comparison between conventional device with capillaries and needles sealed onto the surface of microscope slides (a–c) and a CNC milled device with two Lego®-inspired blocks and stainless-steel tube connectors (d–f): (a) & (d) Photographs of the devices; (b) & (e) Cross-sectional views of tapered-end inner capillary and coaxial outer capillary; (c) & (f) Micrographs of the injection and collection orifice.

glass slides. Ge et al. [22] embedded a double-bore injection capillary into a PMMA cross junction to form Janus droplets. Another glass capillary was inserted in the same junction from the opposite side to collect the produced droplets. Both devices required a lot of manual work for fabrication.

Benson et al. [23] used two commercial PEEK™ chromatography tees to align two round glass capillaries inside a square glass capillary. The device was easy to dismantle and assemble and allowed adjustment of the distance between inner round capillaries during operation by pulling or pushing the capillaries inside the outer capillary. The device was able to generate monodisperse O/W or water-in-oil (W/O) emulsions with a droplet size down to 20 μm. Chang et al. [24] inserted two coaxial capillaries inside two *T*-junction connectors and used the device to make core-shell monomer droplets via two sequential co-flow drop generation steps.

Martino et al. [25] fabricated a glass capillary device by 3D printing acrylonitrile butadiene styrene. The device consisted of a rectangular platform with a square observation hole in the middle and two sliding connectors holding coaxial assembly of round and square capillaries. The distance between inner capillaries could be adjusted during drop generation by moving the connectors along two rails made at both sides of the platform. After 3D printing, the support material must be removed by sonicating the parts with isopropanol. Herranz-Blanco et al. [26] fabricated a glass capillary device with a round-capillary-inside-round-capillary geometry using Shapeways 3D printed steel. The device was used to prepare polymeric nanoparticles by nanoprecipitation and core/shell droplets. Shapeways 3D printed steel is corrosive and non-biocompatible, since it contains 40% bronze, and the printing resolution of 3 mm is relatively poor [27]. Both devices mentioned above are fed with the fluids using hypodermic needles.

Micromilling has advantages over 3D printing in terms of the broader choice of materials that can be used for fabrication, precision, speed, and cleanliness of the finished product [28]. The main disadvantage of all subtractive manufacturing methods including micromilling is the generation of waste during fabrication compared to 3D printing which uses the exact amount of material to make the desired part [29]. Both processes employ computer numerical control (CNC) machining that automates the process and enables direct conversion of CAD models to finished parts, thereby improving repeatability and precision.

In this work, novel, cheap, easy to dismantle and assemble, and reusable glass capillary devices have been fabricated using micromilling (Fig. 1d). Glass capillaries are held between two interchangeable bespoke plastic blocks that can be easily joined together and separated using Lego®-inspired stud-and-tube coupling system (Fig. S1). Three different blocks were combined in different manners to obtain three different flow configurations. The design allows a round-capillary-inside-round-capillary geometry (Fig. 1e) in contrast with round-capillary-inside-square-capillary geometry used in the conventional device (Fig. 1b). Self-alignment of the capillaries was achieved by precise drilling of the mounting holes in both blocks. Adjustment of the distance between inner capillaries while the device is running is another key feature of this design, besides the use of commercial tube connectors instead of hypodermic needles. By careful design and new improvements, the setup time of the novel devices was reduced from ~30 min in manually made capillary devices to just several minutes. In addition, the device is fully accessible from the top and bottom sides, because all fluids are supplied and collected in the longitudinal direction. Due to their flat shape, the building blocks are stackable and can be extended in transverse direction by adding additional units. The effectiveness, versatility, and long-term production stability of the new devices was successfully confirmed by robust synthesis of various microparticles and nanoparticles.

2. Experimental

2.1. Chemicals

2.1.1. Preparation of liposomes and nanoparticles

Cholesterol (≥99%, Sigma-Aldrich Chemicals, Saint Quentin Fallavier, France) and Lipoid® E80 (Lipoid GmbH, Ludwigshafen, Germany, egg yolk lecithin containing 82% phosphatidylcholine and 9% phosphatidylethanolamine) were used to form liposomes. Lipids were dissolved in analytical grade ethanol (Fisher Scientific, UK) and milli-Q water was prepared using a Millipore 185 Milli-Q Plus unit. Hydrogen tetrachloroaurate(III) ($HAuCl_4 \cdot 3H_2O$, ≥99.9% trace metals basis, Sigma-Aldrich, UK) and polyvinylpyrrolidone (PVP K30, $M_w \sim 40{,}000$ g/mol, Sigma Aldrich, UK) were used as gold precursor and capping agent for gold nanoparticles (AuNPs), respectively. A reagent grade crystalline L-ascorbic acid (Sigma-Aldrich, UK) was used as the reducing agent. The pH of the ascorbic acid solution was adjusted with 2 M NaOH (pure, bench reagent) supplied by Fisher Scientific, UK. Silver nanoparticles (AgNPs) were prepared using $AgNO_3$ (ACS reagent grade, >99.9% trace metals basis), tannic acid (ACS reagent grade, ign. residue ≤0.5%), and citric acid (ACS reagent grade, ≥99.5%) supplied by Sigma-Aldrich.

2.1.2. Preparation of emulsions

In W/O/W emulsions, glycerol (99+%, extra pure, Fisher Scientific, UK) was used to modify viscosity, XIAMETER® RSN-0749 resin (a 50/50 mixture of trimethylsiloxysilicate and cyclomethicone, Univar, UK) and poly(vinyl alcohol) (PVA, M_w = 13,000–23,000 g/mol, 87–89% hydrolysed, Sigma-Aldrich, UK) were used as lipophilic and hydrophilic surfactant, respectively. The oil phase was Dow Corning® 200 fluid, 10 cSt (VWR, UK). Nile red (99%, Sigma-Aldrich) and calcein (ultrapure grade, 98%, Sigma-Aldrich) were used for fluorescent labelling. The carrier oil in W/O emulsions was Miglyol® 840 (Sasol, Germany), a propane-1,2-diol diester of caprylic acid (65–80%), capric acid (20–35%), caproic acid (<2%), lauric acid (<2%), and myristic acid (<1%). In some experiments, Eudragit S100 (Evonik, Germany), a pH sensitive copolymer of methacrylic acid and methyl methacrylate (1:2) was dissolved in the aqueous phase and 4-aminobenzoic acid (99%, Acros Organics, UK) was dissolved in Miglyol as a crosslinker.

2.1.3. Preparation of microcrystals

Piroxicam (PRX) (99% purity, anhydrous) was obtained from Hangzhou Hyper Chemicals Limited (Zhejiang, China) was used as a model active, acetone (purity ≥99.98%) supplied from Fisher Scientific (UK) was used as a solvent for PRX and a symmetric triblock copolymer Pluronic® F-127 (bio reagent containing 100 ppm BHT as inhibitor, $M_n \sim 5800$) supplied from Sigma-Aldrich (UK) was used as a stabiliser. Crystals of PRX monohydrate were formed by mixing together 15 g/l of PRX solution in acetone and 2.5 g/l aqueous solution of Pluronic® F-127.

2.2. Experimental equipment

2.2.1. Capillaries

Borosilicate round capillary tubes supplied from World Precision Instruments (UK) with 2.0/1.56 mm and 1.0/0.58 mm OD/ID were used as inner and outer capillaries, respectively. Inner capillaries were pulled using a P-97 micropipette puller (Sutter Instrument Company, USA) and pulled tips were adjusted to the desired orifice size by grazing against abrasive paper. The orifice size was measured using a Narishige MF-830 microforge (Linton Instrumentation, UK). The capillaries were treated with octadecyltrimethoxysilane and 2-[methoxy(polyethyleneoxy)propyl]

trimethoxysilane to render the surface hydrophobic and hydrophilic, respectively.

2.2.2. Lego® blocks

Three different blocks were designed using SolidWorks software (Dassault Systèmes), a solid modelling computer-aided design (CAD) and computer-aided engineering (CAE) computer program and manufactured using a fully automated CNC milling machine (HAAS Automation, model Super Mini, Norwich, UK). The material used for fabrication was polyacetal (polyoxymethylene) copolymer with a density of 1.41 g/cm^3. The drawings of the blocks are shown in Figs. S2–S4 in the supplementary information.

2.2.3. Experimental set-up

Fluids were delivered using 11 Elite syringe pumps (Harvard Apparatus, UK) from SGE gas-tight glass syringes (10 ml, 25 ml, and 50 ml, Sigma-Aldrich, UK) via fine-bore Portex polyethylene medical tubing (1.52 mm OD/0.86 mm ID, Smiths Medicals, UK), and Omnifit® or Super Flangeless™ tube connectors. The device was mounted on the stage of an inverted biological microscope (GXM-XDS-3, GT Vision, UK), as shown in Fig. S5. The microfluidic process was observed and recorded using a Phantom V9.0 high speed camera at a resolution of 576 × 576 pixels. ImageJ program was used to process the video recordings and determine the droplet diameters.

2.2.4. Materials characterisation

The size, D_v and polydispersity index, *PDI* of vesicles and AgNPs were measured by photon correlation spectroscopy using a Delsa™ Nano HC particle analyser (Beckman Coulter, UK). The absorption spectra of AuNPs were recorded using a Perkin Elmer Lambda 35 UV/VIS spectrometer. The mean size of PRX monohydrate crystals was measured using a Beckman Coulter LS130 laser diffraction particle size analyser. The optical images of the crystals were obtained using a Leitz Ergolux optical microscope and SEM images were acquired using a Hitachi model TM3030 benchtop SEM.

2.3. Flow patterns in the device

Fig. 2 shows three different devices assembled from the building blocks shown in Figs. S2–S4. Depending on the miscibility of liquid streams, the device can be operated as a micromixer or droplet generator. A three-phase device mounted on the microscope is shown in Fig. S5. In the next section, we will demonstrate the controllable production of nano- and microparticles and microcrystals in the new devices using different flow configurations.

3. Results and discussion

3.1. Two-phase co-flow

3.1.1. Preparation of liposomes

In these experiments, a solution composed of 20 mg/ml Lipoid® E80 and 5 mg/ml cholesterol dissolved in ethanol was injected through the inner capillary and Milli-Q water was introduced through the annular space between the inner and outer capillary. After injection, ethanol and lipid molecules diffuse into water in the annular region, while water molecules diffuse in the opposite direction. When the solubility limit of the lipids is exceeded, they self-assemble into disk-like bilayer structures, which bend as they grow, and eventually tend to form a spherical vesicle [30]. Under mild shear forces and/or at high concentration, vesicles tend to aggregate into clusters (Fig. 3a). This vesicle aggregation is reversible, but bilayer defects may induce irreversible fusion of bilayers in clusters.

At low flow rates (Fig. 3a), two liquid streams flow side by side with a sharp boundary, heavy vesicle aggregation in the aqueous phase and a high ethanol concentration in the core region. The mixing time of lipids dissolved in the organic stream is: $t_{mix} \backsim D_i^2/D$, where D_i is the orifice diameter of the injection tube and $D = 0.84 \times 10^{-9}$ m^2/s is the diffusion coefficient of ethanol in water [31]. The residence time of the organic stream in the device is: $t_{res} \backsim LD_i^2/Q_o$, where $L \backsim 9$ cm is the length of the collection capillary downstream of the injection point. For efficient mixing, $t_{res} > t_{mix}$ or $L/D_i > Pe$, where *Pe* is the Peclet number. In Fig. 3(a), 350 and $760 L/D_i \backsim Pe \backsim$; thus $t_{res} > t_{mix}$, i.e. a complete mixing was not achieved in the device. In Fig. 3(b), due to high Q_w/Q_o ratio, high concentration gradients were established at the interface, which led to the build-up of transient interfacial tension between ethanol and water stream [32]. As a result, the interface around the injection nozzle acquired a hemispherical shape typical for immiscible liquids in dripping regime. The fusion of bilayers due to heavy vesicle aggregation led to large vesicle sizes of 550–680 nm, as shown in Fig. 3(a).

When fluid flow rates were high (Fig. 3c and d), the interface was extended into a widening jet and a vortex flow was formed around the jet interface. When lipid bilayer fragments (LBFs) bend from a flat disc into a closed sphere, the energy of a LBF first increases due to bending contribution and then decreases as the edges of the bent disc meet and disappear [33]. Energy dissipation of the vortex ring can help to achieve bending of the flat bilayer discs at smaller diameters resulting in smaller vesicles with lower *PDI* [34]. Also, higher flow rates led to better mixing of the two streams leading to larger number of LBFs being formed, which limited their growth. As shown in Fig. 3c and d, an increase in the total flow rate from 37 ml/h to 45 ml/h led to decrease in the vesicle size from 262 to 222 nm. Therefore, the vesicle size was controlled by manipulating hydrodynamic conditions in the device.

3.1.2. Synthesis of AuNPs

Synthesis of AuNPs was achieved by injecting 1 mM $HAuCl_4$ solution containing 1% (w/v) PVP K30 through the injection tube with 100 μm orifice into 20 mM aqueous solution of ascorbic acid at pH = 10.4. The flow rate of ascorbic acid stream was varied from 15 ml/h to 60 ml/h, while the flow rate of $HAuCl_4$ solution was 15 ml/h. As shown in Fig. 4, the size of AuNPs was controlled in the range from 40 nm to 74 nm by adjusting the flow rate of ascorbic acid stream. A decrease in size of the synthesised AuNPs was achieved by increasing the flow rate of ascorbic acid stream, as can be confirmed by the blue-shift in peak absorbance wavelength, λ_{max} [35,36]. A decrease in particle size at higher flow rates of ascorbic acid stream was due to better mixing of the two streams and lower concentration of AgNPs in the product suspension leading to reduced particle agglomeration [35].

3.2. Two-phase counter-current flow focusing

3.2.1. Preparation of W/O emulsions and gel microparticles

W/O emulsions composed of 5 wt% aqueous glycerol solution (ρ_w = 1012 kg/m^3 and μ_w = 1.2 mPa s) dispersed in 2 wt% XIAMETER® RSN-0749 resin in Dow Corning® 200 fluid (ρ_o = 940 kg/m^3 and μ_o = 10.4 mPa s) were generated using counter-current flow focusing geometry. The interfacial tension between the aqueous and oil phase was 29.9 mN/m. As shown in Fig. 5, the droplet size increased when the flow rate ratio Q_c/Q_d decreased from 4.7 to 2.3, but in both cases highly uniform droplets were achieved. Smaller droplets were formed at higher Q_c/Q_d ratio due to higher drag force exerted on the interface by the oil phase [37]. Therefore,

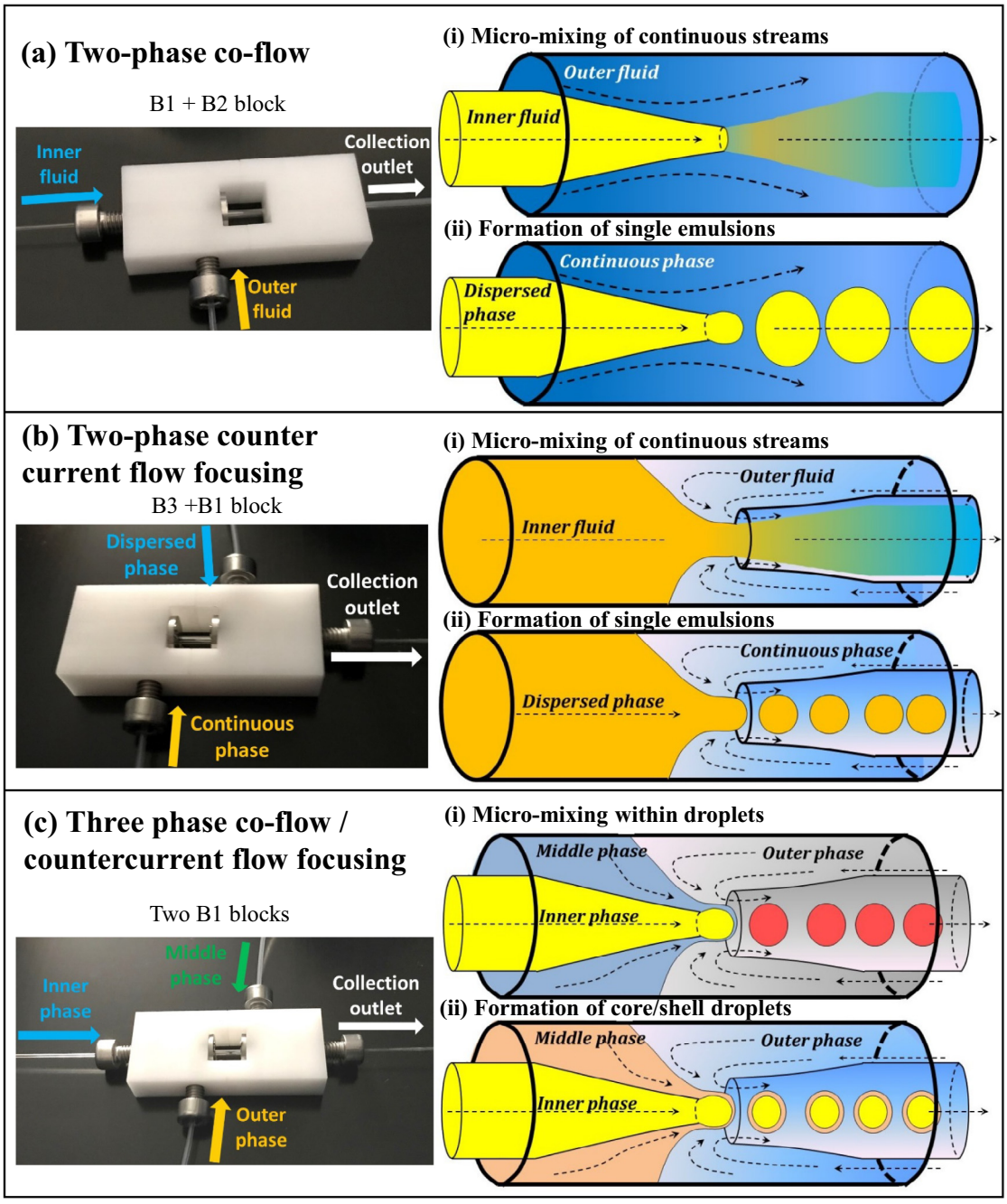

Fig. 2. Three different devices assembled by interlocking different blocks: (a) Two-phase co-flow; (b) Two-phase counter-current flow focusing; (c) Three-phase device combining co-flow and counter-current flow focusing. Interactions between miscible liquid streams lead to micromixing (i), while interactions between immiscible streams lead to drop generation (ii). Micromixing and drop generation can occur in the same device (Figure ci).

the new device was able to generate highly uniform aqueous phase droplets.

To investigate a long-term stability of droplet generation in the flow focusing device, W/O emulsion composed of aqueous Eudragit droplets was formed over 6 h and converted into gel particles. The oil phase was 0.75% (w/v) 4-aminobenzoic acid dissolved in Miglyol 840 and the aqueous phase was 3% (w/v) Eudragit S100 at pH > 7. The device was proven to be stable and leakproof over the entire period of 6 h and enabled consistent generation of monodisperse droplets, as shown in Fig. S6 and Movie 1. After droplet generation, 4-aminobenzoic acid diffused into the droplets due to its high solubility in water of 4.7 g/l at 20 °C and caused the neutralisation of charged carboxylic groups on Eudragit chain, which triggered an internal sol-gel transition of Eudragit S100. 4-Aminobenzoic acid is a relatively weak acid (p*K*a = 2.38) which triggered droplet gelation after jet pinch-off; as a result small gel beads were formed. However, much stronger p-toluenesulfonic acid (p*K*a = −2.8) caused premature gelation of droplets before jet pinch-off, which resulted in large plugs of Eudragit gel [38].

3.2.2. Preparation of drug microcrystals

Microcrystals of PRX monohydrate of controlled size were formed in a flow focusing device by antisolvent crystallisation. A 15 g/l solution of PRX in acetone was delivered at 2 ml/h through

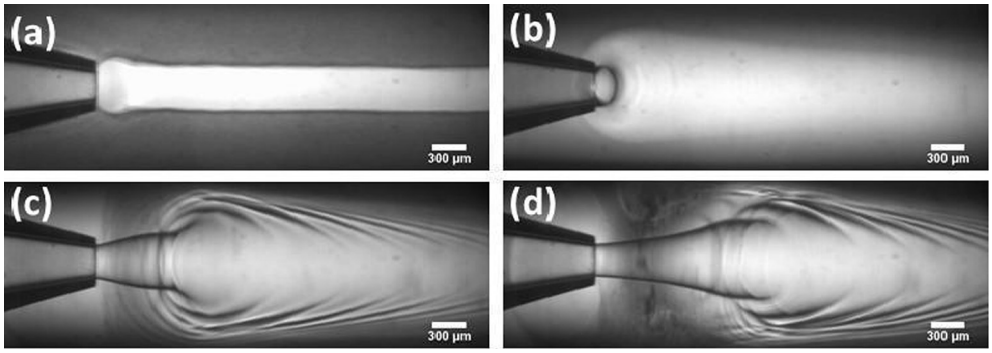

Fig. 3. Fluid streams formed during liposome formation at different organic and aqueous solution flow rates: (a) Q_o = 0.6 ml/h, Q_w = 0.6 ml/h, D_v = 557 nm, *PDI* = 0.245; (b) Q_o = 0.6 ml/h, Q_w = 5 ml/h, D_v = 675 nm, *PDI* = 0.283; (c) Q_o = 12 ml/h, Q_w = 25 ml/h, D_v = 262 nm, *PDI* = 0.145; (d) Q_o = 20 ml/h, Q_w = 25 ml/h, D_v=222 nm, *PDI* = 0.093.

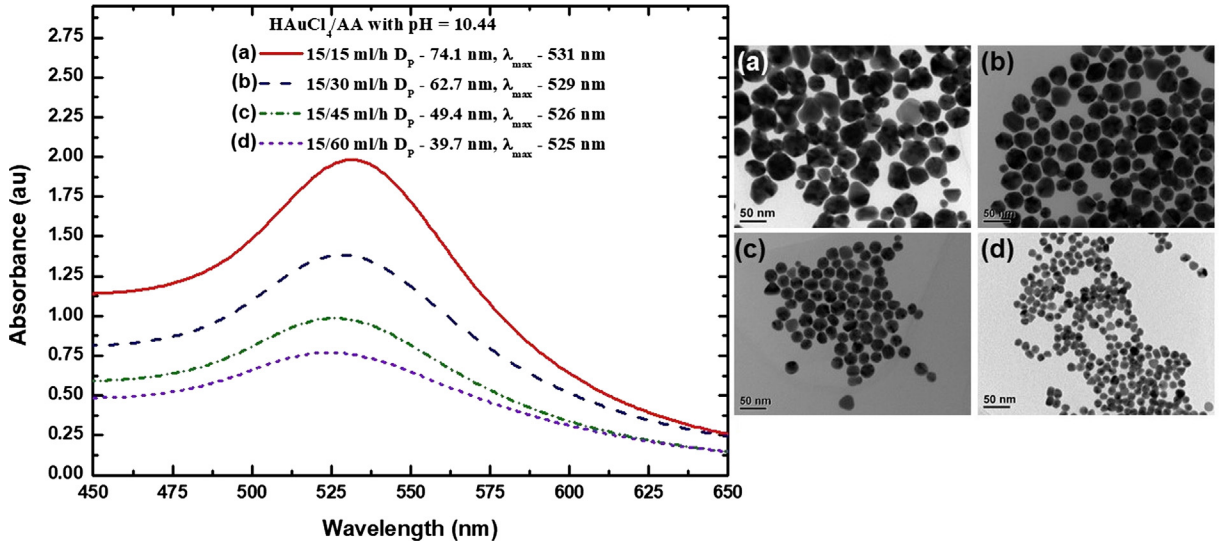

Fig. 4. The effect of flow rate of the ascorbic acid stream on the absorbance spectra, the size of AuNPs, D_p (DLS measurements), and the wavelength of maximum absorbance, λ_{max}, at an orifice diameter of D_i = 100 μm and a flow rate of the $HAuCl_4$ solution of 15 ml/h. The corresponding TEM images of AuNPs are also shown with the number average particle size measured using 100 nanoparticles in each sample: (a) 44 ± 7 nm; (b) 35 ± 4 nm; (c) 23 ± 2 nm; (d) 16 ± 2 nm.

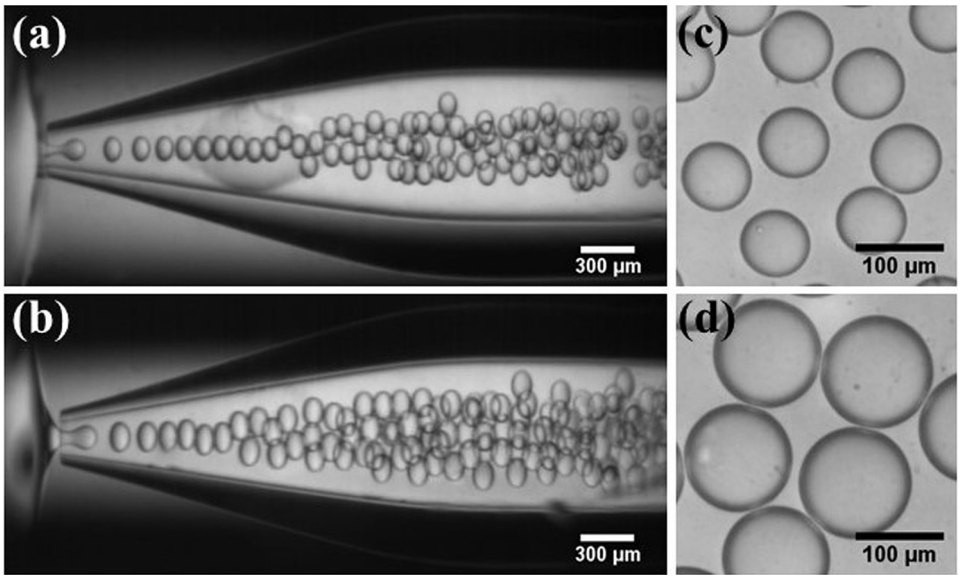

Fig. 5. Formation of W/O emulsions in flow focusing device with D_i = 180 μm: (a) Q_d = 1.9 ml/h, Q_c= 9 ml/h; (b) Q_d = 3 ml/h, Q_c = 7 ml/h. The corresponding droplet diameters and flow rate ratios are: (c) D_d = 80.6 ± 1.3 μm at Q_c/Q_d = 4.7; (d) D_d = 122.8 ± 2.9 μm at Q_c/Q_d = 2.3.

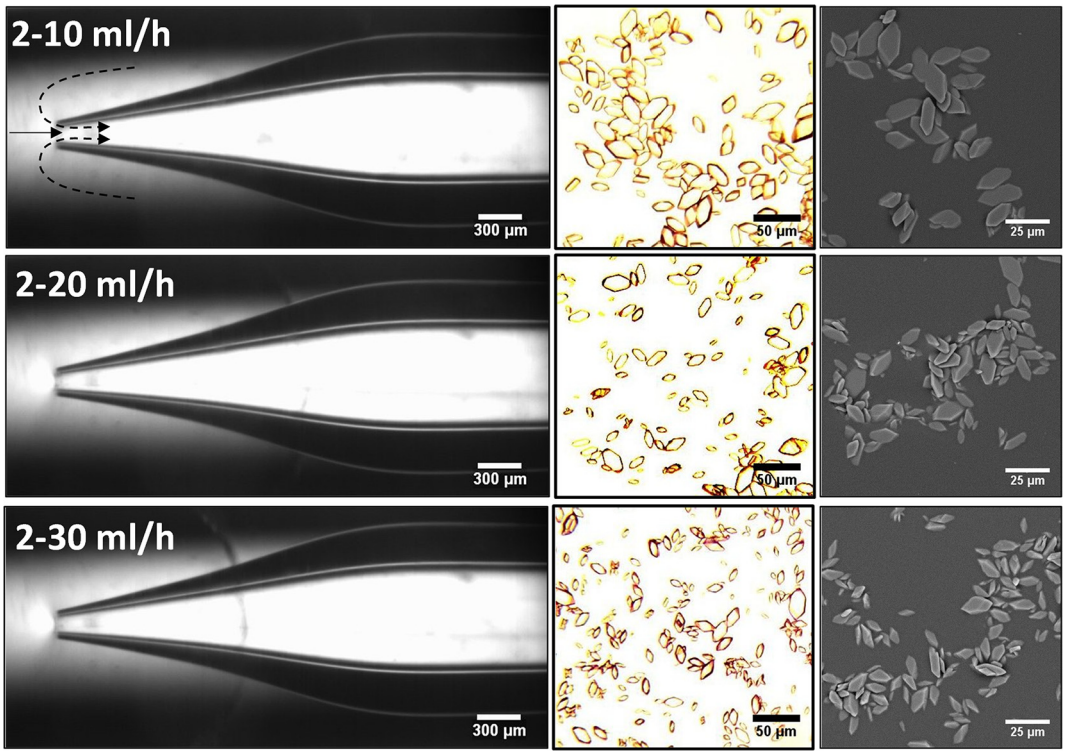

Fig. 6. Preparation of PRX monohydrate crystals in flow focusing device with an orifice size of D_i = 100 µm. A 15 g/l solution of PRX in acetone was delivered at 2 ml/h through the outer capillary from the left-hand side (see, the solid line with an arrow). A 2.5 g/l aqueous solution of Pluronic F-127 was supplied at 10–30 ml/h through the outer capillary from the opposite side of the device (see the dashed arrows). The crystals were formed inside the collection capillary.

the outer capillary at the left-hand side of the device and 2.5 g/l aqueous solution of Pluronic F-127 was supplied through the outer capillary from the opposite side (Fig. 6). The crystals were formed inside the collection capillary due to the supersaturation generated by molecular exchange between the solvent and antisolvent streams. As can be seen, the size of the crystals was controlled by the antisolvent flow rate, which influenced the rate of crystal nucleation. By increasing the antisolvent flow rate from 10 to 20 ml/h, then to 30 ml/h, the size of the crystals was reduced from 29 to 12 µm, then to 10 µm, respectively. By increasing the antisolvent to solvent mass ratio from 5:1 to 15:1, the rate of nucleation increased compared to the rate of crystal growth leading to the formation of large numbers of smaller crystals. Compared to the conventional batch anti-solvent crystallisation methods, microfluidic routes provide superior control of particle size distribution and reduce the batch-to-batch variations by continuous crystallisation approach.

3.3. Three-phase flow

3.3.1. Preparation of multiple emulsions

The inner aqueous phase composed of 5 wt% glycerol (ρ_{ip} = 1012 kg/m^3 and μ_{ip} = 1.2 mPa s), the oil phase composed of 2 wt% XIAMETER® RSN-0749 resin in 98 wt% Dow Corning® 200 fluid (ρ_{mp} = 940 kg/m^3 and μ_{mp} = 10.4 mPa s) and the outer aqueous phase composed of 40 wt% glycerol and 2 wt% PVA (ρ_{op} = 1107 kg/m^3 andμ_{op} = 7.9 mPa s) were used to generate W/O/W emulsions by co-flow combined with counter-current flow focusing. The interfacial tension at the inner and outer interface was 29.9 and 31.8 mN/m, respectively. The ability to self-align capillaries was also investigated as well as the ability to change the distance between inner capillaries while droplets were produced.

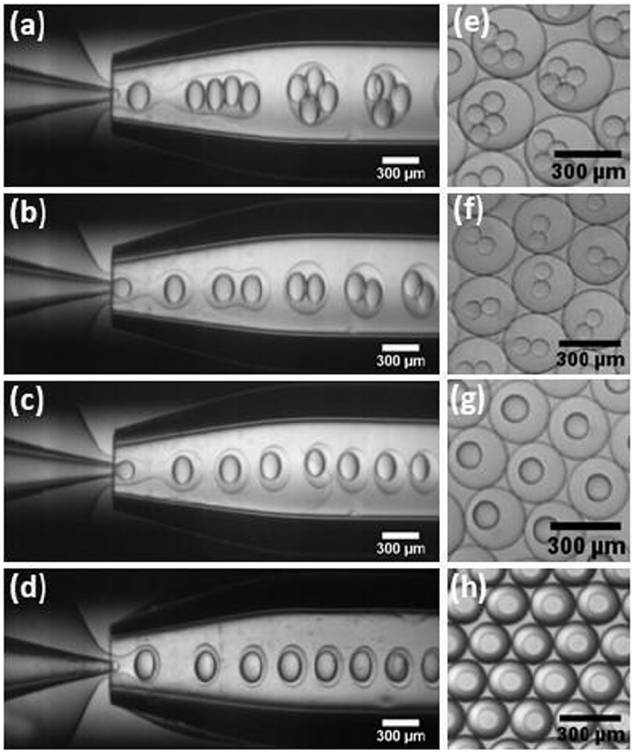

Fig. 7. W/O/W emulsions generated in a three-phase device with D_i = 50 µm and D_c = 300 µm at: (a) Q_{ip} = 4 ml/h, Q_{mp}= 6 ml/h, Q_{op}= 25 ml/h, quadruple core encapsulation; (b) Q_{ip} = 2.5 ml/h, Q_{mp}= 6 ml/h, Q_{op}= 25 ml/h, double core encapsulation; (c) Q_{ip} = 2 ml/h, Q_{mp}= 6 ml/h, Q_{op}= 25 ml/h, single core encapsulation; (d) Q_{ip} = 2 ml/h, Q_{mp} = 3 ml/h, Q_{op}= 20 ml/h, single core in a thin shell. (e), (f), (g), and (h) are the micrographs of generated droplets. Eccentric position of some cores was due to density mismatch between the core and shell fluids.

Fig. 7 shows that the new device self-aligns the capillaries precisely along the main axis and generate stable flows to make double emulsion droplets with single and multiple cores. The number of aqueous cores in each oil drop was changed from 4 to 2 to 1 by decreasing the inner phase flow rate from 4 to 2.5 to 2 ml/h at constant flow rates of the middle and outer fluids, as found earlier in the standard device [39]. It was possible to manipulate the shell thickness and the core size by changing the inner phase to middle phase flow rate ratio, Q_{ip}/Q_{mp}. It was also possible to encapsulate calcein (highly hydrophilic dye) in the core fluid and Nile red (highly hydrophobic dye) in the shell fluid and to achieve 100% encapsulation efficiency of both dyes (Fig. 8). The encapsulation efficiency of the fluorescent dyes was determined by measuring the fluorescent intensities of dyes in the oil phase and aqueous phase. Therefore, the new device can be used to simultaneously encapsulate hydrophilic and hydrophobic actives with high efficiency.

The new device has the ability to move the injection capillary backward and forward inside the square capillary and thus to change the distance ΔL between the two inner capillary tubes while the experiment is running, as shown in Fig. 9 and Movie 2. ΔL has a negative value in Fig. 9 when the end of the injection tube is placed upstream of the inlet section of the collection tube. The minimum drop size was achieved when $\Delta L/D_c = 0$, i.e. when the outlet section of the injection tube coincided with the inlet section of the collection tube. The size of core/shell droplets was successfully manipulated at constant fluid flow rates by gradually changing ΔL from $-0.8D_c$ to zero. Shear force exerted on the outer interface depends on the position of the injection tube. The shear force has the maximum value at the inlet section of the collection tube due to smallest cross-sectional area and the highest velocity of the outer fluid. Furthermore, by pushing the injection tube inside the collection tube to achieve $\Delta L > 0$, it was possible to produce double core droplets and to adjust their size. The greater the ΔL value, the larger the size of the generated inner and outer drops, due to increasingly smaller shear [40].

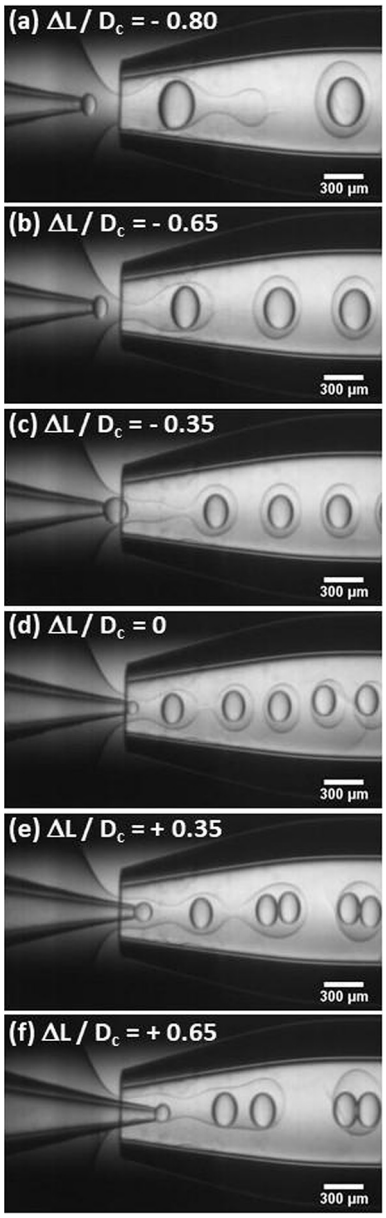

Fig. 9. The effect of the distance ΔL between the injection and collection capillary orifice on the morphology of W/O/W emulsion droplets formed at Q_{ip} = 2 ml/h, Q_{mp} = 6 ml/h, Q_{op} = 25 ml/h, D_i = 50 µm, and D_c = 300 µm.

3.3.2. Preparation of silver nanoparticles (AgNPs)

Three-phase device can be used for mixing two miscible streams within droplets (Fig. 2ci), which will be demonstrated by the green synthesis of AgNPs within aqueous droplets formed in an inert and environmentally friendly oil. The process involves merging together 3.125 mM solution of silver nitrate delivered through the injection tube and 10 mM aqueous 1:1 tannic acid and sodium citrate solution at pH ≈ 10 delivered co-currently through the outer capillary. The formed mixture was flow focused by Miglyol 840 delivered from the opposite side of the outer

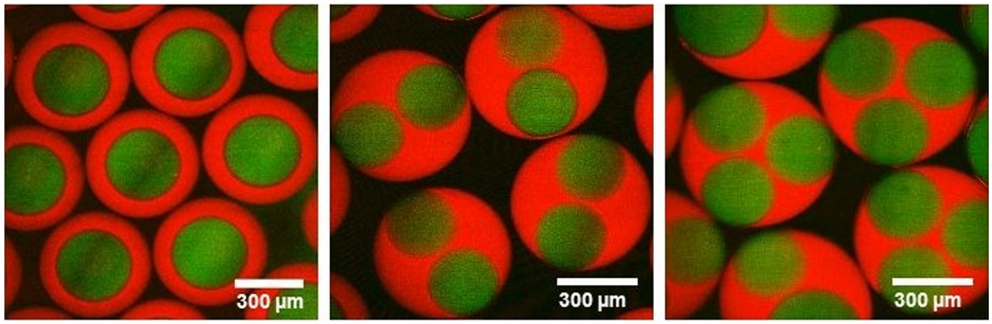

Fig. 8. W/O/W emulsion droplets with calcein and Nile red encapsulated in the core and shell fluid respectively: (a) core-shell droplets with the core diameter of 258 ± 4 µm and the shell diameter of 391 ± 7 µm; (b) double-core multiple emulsion droplets with the core diameter of 240 ± 8 µm and the shell diameter of 503 ± 9 µm; (c) triple-core multiple emulsion droplets with the core diameter of 251 ± 3 µm and the shell diameter of 550 ± 8 µm.

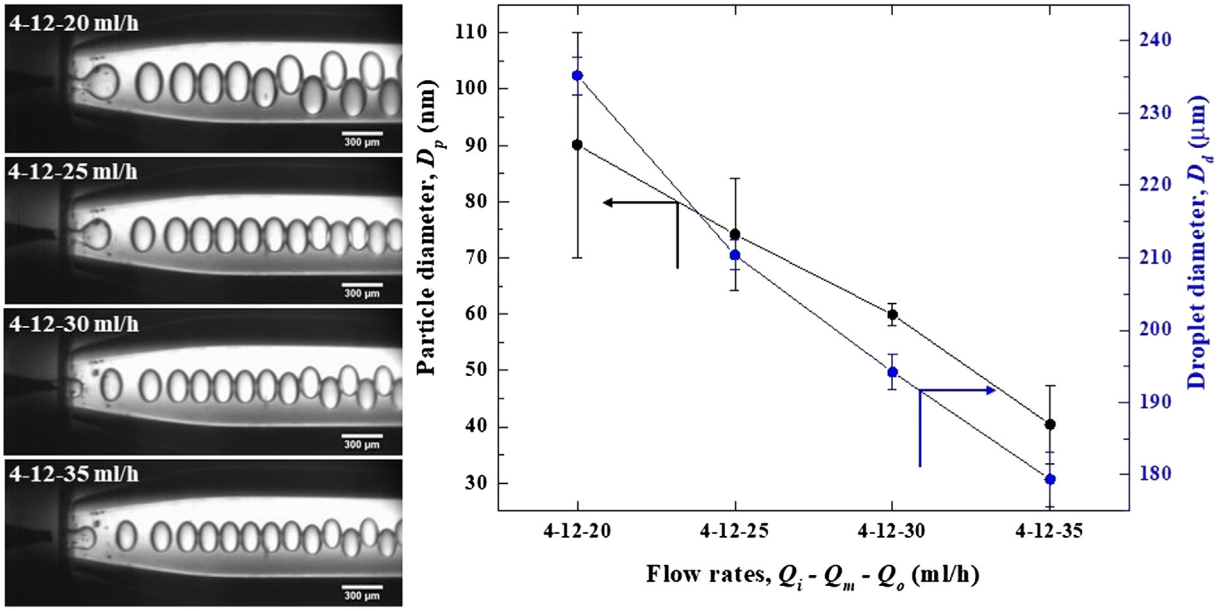

Fig. 10. Preparation of AgNPs within droplets by mixing 3.125 mM aqueous $AgNO_3$ solution and 10 mM aqueous 1:1 tannic acid and trisodium citrate solution. The flow rate of Miglyol 840 varied from 20 to 25 to 30 to 35 ml/h, while the flow rates of $AgNO_3$ and tannic acid streams were fixed at 4 ml/h and 12 ml/h, respectively. Injection and collection capillary orifice diameters were 50 µm and 300 µm respectively.

capillary, which resulted in the generation of droplets that underwent chemical reaction in the collection tube. At alkaline pH, tannic acid hydrolyses into glucose and gallic acid and gallic acid induces reduction of Ag^+ ions and formation of AgNPs at room temperature [41]. Sodium citrate provides the ionic stabilisation to the AgNPs produced. The size of the synthesized AgNPs was precisely controlled by the size of the reaction droplets, as shown in Fig. 10. Smaller NPs were formed using higher oil flow rates, due to higher internal fluid circulation and more vigorous mixing within droplets. The advantage of 3-phase device over 2-phase device with two parallel reactant streams is that the reaction mixture is isolated from the walls of the collection tube, which prevents deposition of the NPs onto the walls.

4. Conclusions

Novel, reconfigurable, reusable, cost-effective, and user-friendly glass capillary devices composed of Lego® inspired building blocks have been fabricated using CNC milling and successfully used for production of nanoparticles and droplets of controllable size in co-flow, counter-current flow focusing and three-phase flow configurations. The new devices were proved to be reliable, leak free, easy to dismantle and reassemble, as well as robust for multiple and extended usage compared to traditional disposable glass capillary devices [4]. Various applications were tested to demonstrate the versatility and robustness of the device. The distance between the inner capillaries can be manipulated during operation, which have a profound effect on fluid micromixing and jet break-up processes. The device could potentially be improved by incorporating a mechanism that would enable a precise movement of the injection tube. Mixing in two-dimensional viscous flow within a microchannel is inherently inefficient. One of the flow patterns of the new device that overcome this obstacle and prevent deposition of the generated nanomaterials on the channel walls was co-flow combined with counter-current flow focusing, resulting in vigorous shear-induced mixing of reactant streams within droplets and formation of nanoparticles.

Scaling up microfluidic devices to meet the industrial scale production demands is one of the pressing needs of the microfluidic research community [42]. Romanowsky et al. [43] developed and tested parallelized PDMS microfluidic devices consisted of 8 or more double drop makers. The scalability was also proven in continuous pharmaceutical manufacturing where several parallel microfluidic devices were successfully operated and tightly controlled alongside more conventional processes such as millifluidic tubular reactors and continuous filtration processes [2,44,45]. Capillary devices with parallelized coaxial capillary assemblies are yet to be designed and tested.

To meet the demand of scaling up microfluidics, one option to parallelize the Lego® inspired glass capillary devices is to place several different blocks horizontally or vertically and provide common tube connectors for all of them. In addition, the new design opens up opportunities to attach additional blocks, which can be locked using the same mechanism, upstream or downstream of the drop generation block. These additional blocks can also be used to embed a portable UV light source, a fluorescence detection system, Peltier heating and cooling elements, interdigital transducers, micro-analytical tools and other detectors. Lego®-inspired blocks developed here can be modified to incorporate additional flow streams and achieve simultaneous interaction of more than 3 different fluids within the device [7,9,12] which are some of the future plans of the authors.

Acknowledgements

The authors acknowledge the financial support for this work from the Enterprise Projects Group (EPG) of Loughborough University, grant 18/14606. The authors would also like to thank Mr Tony Eyre and Mr Steven Bowler from the Chemical Engineering Department in Loughborough for their contribution in manufacturing the glass capillary holders using CNC machining and LMCC for TEM images. The experimental set-up was provided from the UK Engineering and Physical Sciences Research Council (EPSRC) grant EP/HO29923/1.

Appendix A. Supplementary material

Supplementary data to this article can be found online at https://doi.org/10.1016/j.jcis.2019.01.119.

References

[1] G.M. Whitesides, The origins and the future of microfluidics, Nature 442 (2006) 368–373, https://doi.org/10.1038/nature05058.
[2] S. Mascia, P.L. Heider, H. Zhang, R. Lakerveld, B. Benyahia, P.I. Barton, B.L. Trout, End-to-end continuous manufacturing of pharmaceuticals: integrated synthesis, purification, and final dosage formation, Angew. Chem., Int. Ed. 125 (2013) 12585–12589, https://doi.org/10.1002/ange.201305429.
[3] B. Benyahia, Applications of a plant-wide dynamic model of an integrated continuous pharmaceutical plant: design of the recycle in the case of multiple impurities, in: R. Singh, Z. Yuan (Eds.), Process Systems Engineering for Pharmaceutical Manufacturing: From Product Design to Enterprise-Wide Decisions, Comput.-Aided Chem. Eng., 41 (2018) pp. 141–157. doi: 10.1016/B978-0-444-63963-9.00006-3.
[4] A.S. Utada, E. Lorenceau, D.R. Link, P.D. Kaplan, H.A. Stone, D.A. Weitz, Monodisperse double emulsions generated from a microcapillary device, Science 308 (2005) 537–541, https://doi.org/10.1126/science.1109164.
[5] L.Y. Chu, H.C. Shum, A. Fernandez-Nieves, A.S. Utada, E.S. Carreras, D.A. Weitz, Emulsions and techniques for formation, UP Patent US7776927B2, 2010.
[6] S. Takeuchi, P. Garstecki, D.B. Weibel, G.M. Whitesides, An axisymmetric flow-focusing microfluidic device, Adv. Mater. 17 (2005) 1067–1072, https://doi.org/10.1002/adma.200401738.
[7] L. Shang, Y. Cheng, J. Wang, H. Ding, F. Rong, Y. Zhao, Z. Gu, Double emulsions from a capillary array injection microfluidic device, Lab Chip 14 (2014) 3489–3493, https://doi.org/10.1039/c4lc00698d.
[8] S.H. Kim, D.A. Weitz, One-step emulsification of multiple concentric shells with capillary microfluidic devices, Angew. Chem., Int. Ed. 50 (2011) 8731–8734, https://doi.org/10.1002/anie.201102946.
[9] L.L.A. Adams, T.E. Kodger, S.H. Kim, H.C. Shum, T. Franke, D.A. Weitz, Single step emulsification for the generation of multi-component double emulsions, Soft Matter 8 (2012) 10719–10724, https://doi.org/10.1039/c2sm25953b.
[10] W.J. Duncanson, A. Abbaspourrad, H.C. Shum, S.H. Kim, L.L.A. Adams, D.A. Weitz, Monodisperse gas-filled microparticles from reactions in double emulsions, Langmuir 28 (2012) 6742–6745, https://doi.org/10.1021/la300915p.
[11] G.T. Vladisavljević, Recent advances in the production of controllable multiple emulsions using microfabricated devices, Particuology 24 (2016) 1–17, https://doi.org/10.1016/j.partic.2015.10.001.
[12] L.Y. Chu, A.S. Utada, R.K. Shah, J.W. Kim, D.A. Weitz, Controllable monodisperse multiple emulsions, Angew. Chem., Int. Ed. 46 (2007) 8970–8974, https://doi.org/10.1002/anie.200701358.
[13] W. Wang, R. Xie, X.J. Ju, T. Luo, L. Liu, D.A. Weitz, L.Y. Chu, Controllable microfluidic production of multicomponent multiple emulsions, Lab Chip 11 (2011) 1587–1592, https://doi.org/10.1039/c1lc20065h.
[14] W. Wang, M.J. Zhang, R. Xie, X.J. Ju, C. Yang, C.L. Mou, D.A. Weitz, L.Y. Chu, Hole-shell microparticles from controllably evolved double emulsions, Angew. Chem., Int. Ed. 52 (2013) 8084–8087, https://doi.org/10.1002/anie.201301590.
[15] W. Wang, M.J. Zhang, L.Y. Chu, Microfluidic approach for encapsulation via double emulsions, Curr. Opin. Pharmacol. 18 (2014) 35–41, https://doi.org/10.1016/j.coph.2014.08.003.
[16] S.H. Kim, J.W. Kim, J.C. Cho, D.A. Weitz, Double-emulsion drops with ultra-thin shells for capsule templates, Lab Chip 11 (2011) 3162–3166, https://doi.org/10.1039/c1lc20434c.
[17] G.T. Vladisavljević, I. Kobayashi, M. Nakajima, Production of uniform droplets using membrane, microchannel and microfluidic emulsification devices, Microfluid. Nanofluid. 13 (2012) 151–178, https://doi.org/10.1007/s10404-012-0948-0.
[18] G.S. Fiorini, D.T. Chiu, Disposable microfluidic devices: Fabrication, function, and application, Biotechniques 38 (2005) 429–446, https://doi.org/10.2144/05383RV02.
[19] J.N. Lee, C. Park, G.M. Whitesides, Solvent compatibility of poly (dimethylsiloxane)-based microfluidic devices, Anal. Chem. 75 (2003) 6544–6554, https://doi.org/10.1021/ac0346712.
[20] R.M. Van Dam, Solvent-resistant elastomeric microfluidic devices and applications, California Institute of technology, PhD Thesis, 2006. <http://thesis.library.caltech.edu/4796/3/02_Chapter_2.pdf>.
[21] E.Q. Li, J.M. Zhang, S.T. Thoroddsen, Simple and inexpensive microfluidic devices for the generation of monodisperse multiple emulsions, J. Micromech. Microeng. 24 (2014) 15019, https://doi.org/10.1088/0960-1317/24/1/015019.
[22] X.H. Ge, J.P. Huang, J.H. Xu, J. Chen, G.S. Luo, Water–oil janus emulsions: microfluidic synthesis and morphology design, Soft Matter 12 (2016) 3425–3430, https://doi.org/10.1039/c6sm00130k.
[23] B.R. Benson, H.A. Stone, R.K. Prud'homme, An "off-the-shelf" capillary microfluidic device that enables tuning of the droplet breakup regime at constant flow rates, Lab Chip 13 (2013) 4507–4511, https://doi.org/10.1039/c3lc50804h.
[24] Z. Chang, C.A. Serra, M. Bouquey, L. Prat, G. Hadziioannou, Co-axial capillaries microfluidic device for synthesizing size- and morphology-controlled polymer core-polymer shell particles, Lab Chip 9 (2009) 3007–3011, https://doi.org/10.1039/b913703c.
[25] C. Martino, S. Berger, R.C.R. Wootton, A.J. DeMello, A 3D-printed microcapillary assembly for facile double emulsion generation, Lab Chip 14 (2014) 4178–4182, https://doi.org/10.1039/c4lc00992d.
[26] B. Herranz-Blanco, E. Ginestar, H. Zhang, J. Hirvonen, H.A. Santos, Microfluidics platform for glass capillaries and its application in droplet and nanoparticle fabrication, Int. J. Pharm. (2017) 100–105, https://doi.org/10.1016/j.ijpharm.2016.11.024.
[27] Shapeways, Stainless Steel 3D Printing Material Information - Shapeways, 2018. <https://www.shapeways.com/materials/steel> (accessed 05.05.17).
[28] C.R. Friedrich, M.J. Vasile, Development of the micromilling process for high-aspect-ratio microstructures, J. Microelectromech. Syst. 5 (1996) 33–38, https://doi.org/10.1109/84.485213.
[29] D.J. Guckenberger, T. de Groot, A.M.D. Wan, D. Beebe, E. Young, Micromilling: A method for ultra-rapid prototyping of plastic microfluidic devices, Lab Chip 15 (2015) 2364–2378, https://doi.org/10.1039/C5LC00234F.
[30] C. Huang, D. Quinn, Y. Sadovsky, S. Suresh, K.J. Hsia, Formation and size distribution of self-assembled vesicles, Proc. Natl. Acad. Sci. 114 (2017) 2910–2915, https://doi.org/10.1073/pnas.1702065114.
[31] E.L. Cussler, Diffusion Mass Transfer in Fluid Systems, 2009.
[32] L. Lacaze, P. Guenoun, D. Beysens, M. Delsanti, P. Petitjeans, P. Kurowski, Transient surface tension in miscible liquids, Phys. Rev. E - Stat. Nonlinear, Soft Matter Phys. 82 (2010) 1–8, https://doi.org/10.1103/PhysRevE.82.041606.
[33] S.M. Phapal, P. Sunthar, Influence of micro-mixing on the size of liposomes self-assembled from miscible liquid phases, Chem. Phys. Lipids 172–173 (2013) 20–30, https://doi.org/10.1016/j.chemphyslip.2013.04.006.
[34] G.T. Vladisavljević, A. Laouini, C. Charcosset, H. Fessi, H.C.H. Bandulasena, R.G. Holdich, Production of liposomes using microengineered membrane and co-flow microfluidic device, Colloids Surf. A 458 (2014) 168–177, https://doi.org/10.1016/j.colsurfa.2014.03.016.
[35] M.V. Bandulasena, G.T. Vladisavljević, O.G. Odunmbaku, B. Benyahia, Continuous synthesis of PVP stabilized biocompatible gold nanoparticles with a controlled size using a 3D glass capillary microfluidic device, Chem. Eng. Sci. 171 (2017) 233–243, https://doi.org/10.1016/j.ces.2017.05.035.
[36] F.Y. Alzoubi, J.Y. Alzouby, M.K. Alqadi, H.A. Alshboul, K.M. Aljarrah, Synthesis and characterization of colloidal gold nanoparticles controlled by the pH and ionic strength, Chin. J. Phys. 53 (2015) 100801–100809, https://doi.org/10.6122/CJP.20150601E.
[37] E.E. Ekanem, S.A. Nabavi, G.T. Vladisavljevic, S. Gu, Structured biodegradable polymeric microparticles for drug delivery produced using flow focusing glass microfluidic devices, ACS Appl. Mater. Interfaces 7 (2015) 23132–23143, https://doi.org/10.1021/acsami.5b06943.
[38] G.K. Vinner, G.T. Vladisavljević, M.R.J. Clokie, D.J. Malik, Microencapsulation of Clostridium difficile specific bacteriophages using microfluidic glass capillary devices for colon delivery using pH triggered release, PLoS One 12 (2017) 1–27, https://doi.org/10.1371/journal.pone.0186239.
[39] S.A. Nabavi, G.T. Vladisavljević, V. Manovic, Mechanisms and control of single-step microfluidic generation of multi-core double emulsion droplets, Chem. Eng. J. 322 (2017) 140–148, https://doi.org/10.1016/j.cej.2017.04.008.
[40] S.A. Nabavi, G.T. Vladisavljević, M.V. Bandulasena, O. Arjmandi-Tash, V. Manović, Prediction and control of drop formation modes in microfluidic generation of double emulsions by single-step emulsification, J. Colloid Interface Sci. 505 (2017) 315–324, https://doi.org/10.1016/j.jcis.2017.05.115.
[41] T. Ahmad, Reviewing the tannic acid mediated synthesis of metal nanoparticles, J. Nanotechnol. 2014 (2014) 954206, https://doi.org/10.1155/2014/954206.
[42] G.T. Vladisavljević, N. Khalid, M.A. Neves, T. Kuroiwa, M. Nakajima, K. Uemura, S. Ichikawa, I. Kobayashi, Industrial lab on a chip: design, applications and scale up for drug discovery and delivery, Adv. Drug Deliv. Rev. 65 (2013) 1626–1663, https://doi.org/10.1016/j.addr.2013.07.017.
[43] M.B. Romanowsky, A.R. Abate, A. Rotem, C. Holtze, D.A. Weitz, High throughput production of single core double emulsions in a parallelized microfluidic device, Lab Chip 12 (2012) 802–807, https://doi.org/10.1039/c2lc21033a.
[44] B. Benyahia, R. Lakerveld, P.I. Barton, A plant-wide dynamic model of a continuous pharmaceutical rocess, Ind. Eng. Chem. Res. 51 (2012) 15393–15412, https://doi.org/10.1021/ie3006319p.
[45] L. Heider, S.C. Born, S. Basak, B. Benyahia, R. Lakerveld, H. Zhang, R. Hogan, L. Buchbinder, A. Wolfe, S. Mascia, J.M.B. Evans, T.F. Jamison, K.F. Jensen, Development of a multi-step synthesis and workup sequence for an integrated, continuous manufacturing process of a pharmaceutical, Org. Process Res. Dev. 18 (2014) 402–409, https://doi.org/10.1021/op400294z.